Nanodrug delivery system targeting FAP for the combined treatment of oral leukoplakia

Ran Li (lraner@163.com)
Shanxi Province Key Laboratory of Oral Diseases Prevention and New Materials Shanxi Medical University School and Hospital of Stomatology https://orcid.org/0000-0002-0647-2557

Yingjiao Zhao
Shanxi Province Key Laboratory of Oral Diseases Prevention and New Materials,Shanxi Medical University School and Hospital of Stomatology

Tiantian Liu
Shanxi Province Key Laboratory of Oral Diseases Prevention and New Materials,Shanxi Medical University School and Hospital of Stomatology

Yanwei Li
Shanxi Province Key Laboratory of Oral Diseases Prevention and New Materials,Shanxi Medical University School and Hospital of Stomatology

Chaoqiong Wan
Shanxi Province Key Laboratory of Oral Diseases Prevention and New Materials,Shanxi Medical University School and Hospital of Stomatology

Ruifang Gao
Shanxi Province Key Laboratory of Oral Diseases Prevention and New Materials,Shanxi Medical University School and Hospital of Stomatology

Chen Liu
Shanxi Province Key Laboratory of Oral Diseases Prevention and New Materials,Shanxi Medical University School and Hospital of Stomatology

Xianqi Li
Shanxi Province Key Laboratory of Oral Diseases Prevention and New Materials Shanxi Medical University School and Hospital of Stomatology

Bing Li
Shanxi Province Key Laboratory of Oral Diseases Prevention and New Materials Shanxi Medical University School and Hospital of Stomatology

Research Article

Keywords: Nanomedicine, photodynamic therapy, oral leukoplakia, drug therapy, targeted therapy

Posted Date: April 17th, 2023

DOI: https://doi.org/10.21203/rs.3.rs-2776517/v1

Version of Record: A version of this preprint was published at Drug Delivery and Translational Research on August 1st, 2023. See the published version at https://doi.org/10.1007/s13346-023-01397-6.

Abstract

Oral leukoplakia (OLK) has received much attention due to its potential risk of malignant transformation. Studies have shown that when drug therapy is combined with photothermal therapy (PTT), not only can the cytotoxicity of the drug be enhanced, but also the heat energy can be used to kill the lesion cells, so we can combine drug therapy with PTT to enhance the therapeutic effect on OLK. However, with certain drawbacks due to its lack of targeting, fibroblast activating protein (FAP) has become an attractive target for OLK combination therapy. In this study, we used NGO-PEG loaded with FAP-targeting peptide and celecoxib (CXB) to construct a nano-drug delivery system CGPF for targeting OLK with high FAP expression, and confirmed the biocompatibility and therapeutic efficacy of CGPF by in vitro and in vivo experiments. Overall, the novel nano-drug delivery system CGPF proposed in this study showed a very significant potential for the combination therapy of OLK.

Introduction

Oral leukoplakia (OLK) is one of the most common oral potentially malignant diseases (OPMDs) in the oral mucosa, with a malignancy rate of 0.13-34.0%[1, 2]. The main methods of treating OLK in clinical practice are surgical excision, freezing, laser and drug therapy, but all of these methods are inadequate. Restricted by the special anatomical structure and functional needs of the oral and maxillofacial region, certain areas are not suitable for surgical, cryotherapy and laser treatment. And the treatment process cannot accurately locate the edges of the diseased tissue, resulting in residual malignant leukoplakic tissue[3, 4].Topical application of drugs, which also has the problem of edge determination, can only be effective for the extent of lesions visible to the naked eye, but cannot completely eradicate the already mutated cells present outside the lesion area. If systemic administration is used, the lack of targeting leads to reduced bioavailability of the drug and can produce greater systemic toxicities[5, 6].To reduce these drawbacks, combining different therapeutic approaches, i.e., combination therapy, offers new opportunities for OLK treatment. Current studies have shown that when drug therapy is combined with thermotherapy, not only can the cytotoxicity of the drug be enhanced, but also the heat can be used to kill the diseased cells and improve the efficacy[7, 8]. Photothermal therapy (PTT), as a kind of thermal therapy, plays an indispensable role in the treatment of OLK, so we can combine drug therapy with PTT to enhance the therapeutic effect on OLK[9]. However, PTT lacks specificity to the lesion site and often causes unavoidable thermal damage to the normal tissues and organs surrounding the lesion. In view of the above, finding the target site for the combination therapy of OLK is crucial.

Fibroblast activating protein (FAP) has become an attractive target as a hotspot in recent years[10].FAP belongs to a group of type II transmembrane glycoproteins that are highly expressed in tumors of epithelial origin, such as breast, pancreatic and oral squamous cell carcinomas, as well as in inflammatory diseases, while they are hardly expressed in normal adult tissues[11–16]. The progression from OLK to oral squamous cell carcinoma (OSCC) involves a complex inflammatory process[17]. Based on this we conjectured that FAP is highly expressed in OLK. sequencing data by Debodipta Das et al. confirmed our conjecture that FAP expression is significantly different in OLK and normal mucosal

tissues[18].Currently, no reports have been found for targeting FAP for OLK combination therapy. Based on the above research background and current problems, we can use FAP as a target to find a nanocarrier with high photothermal conversion efficiency and high photothermal stability and construct a nanosystem to combine drug therapy and PTT to improve the treatment effect of oral leukoplakia.

Good biocompatibility, good passive targeting, easy and efficient transport into cells, protection of peptides or DNA from enzymatic cleavage, high fluorescence quenching efficiency, and good photothermal conversion efficiency make graphene oxide nanoparticles (NGO) of great interest in therapeutic areas[19–24].NGO is the oxidized form of graphene and consists of a network of hexagonal cyclic carbon with abundant oxygen-containing functional groups that provide covalent and non-covalent reactions to load functional molecules providing rich active centers[25–28].In addition the high surface area associated with the presence of oxygen-containing groups allows for the loading of a wide range of molecules [29, 30].By targeting ligands and drug loading, NGO can be used for drug therapy and PTT targeting of diseased cells for higher therapeutic efficacy.

Here, we designed and synthesized a multifunctional NGO conjugate to combine pharmacotherapy with PTT for the treatment of OLK.In this study, we relied on cellular and human oral mucosa specimens to verify the high expression of FAP in OLK using cellular immunochemical and immunohistochemical assays. Then, we used amidated PEG to modify the surface of NGO by amide reaction with it to obtain PEGylated NGO with better biocompatibility and stability[31, 32].And it was used as a carrier to adsorb FAP targeting peptides and cyclooxygenase-2 (Cyclooxygenase-2) enzyme inhibitors via hydrogen and π-π bonds **Scheme. 1** Synthesis of the nano-drug delivery system and description of the combined photothermal treatment strategy(Scheme. 1).In addition, its targeting ability and therapeutic efficacy were evaluated in vitro and in vivo, and the system was able to target DOK cells with high FAP expression and OLK through ligand-receptor interactions, and the combined efficacy of drug therapy and PTT was greatly improved after combined treatment. The combined efficacy of drug therapy and PTT was greatly improved, providing a new method and theoretical basis for OLK diagnosis and treatment.

Materials And Methods

Materials

SABC-POD kit, phosphate-buffered saline (PBS), CCK8 reagent, DAPI staining solution, and anti-fluorescence attenuation blocker were purchased from Dr. D.

The FAP antibody was purchased from ABCAM, DAB; color development kit from Nakasugi Golden Bridge; and Mayer’s hematoxylin from Regen.

Neutralized gum was purchased from Solaibao; DMEM high sugar and RPMI 1640 medium from GIBCO; selected superior fetal bovine serum from Cellmax; NGO-COOH from Centaur Nano; PEG$(NH_2)_2$ from Yan Yi Bio; FAP-targeting peptide from C-Peptide Biochemistry; 1-(3-dimethylaminopropyl)-3-ethylcarbodiimide

hydrochloride (EDC-HCL) from Maclean; celecoxib, penicillin–streptomycin solution, 0.25% trypsin (EDTA), 4-nitroquinoline-N-oxide (4-NQO), dimethyl sulfoxide (DMSO), serum-free non-programmed cell lyophilization solution (protein-free), and tissue fixative from Mellen; anhydrous ethanol from Tianjin Zhiyuan Chemical Reagent Co.; Triton X-100 from Solarbio; and chloral hydrate from Kermel.

Immunohistochemical Analysis Of Tissue

The study was approved by the Ethics Committee of Shanxi Medical University (2021SLL027), and all experimental protocols and methods were performed in accordance with relevant guidelines and regulations and in compliance with the principles of the Declaration of Helsinki. Written informed consent was signed by all participants.Paraffin-embedded OLK and normal oral mucosa(NOM) tissue specimens were cut into 4-μm sections that were incubated with 5% bovine serum albumin and anti-FAP antibody overnight at 4℃. The slides were incubated with secondary antibodies for 30 min at 37℃. The slides were then observed under an inverted fluorescence microscope (Olympus, Osaka, Japan).

Immunochemical Analysis Of Cells

After the cell slides were fixed, 5% bovine serum albumin and anti-FAP antibody were added dropwise and the samples were incubated at 4℃ overnight. The slides were and incubated with secondary antibodies for 30 min at 37℃. After DAB staining staining, dehydrate and seal the slides and observe them under an inverted fluorescent microscope.

Synthesis And Characterization Of Targeted Nano-probes And Nano-drug Delivery Systems

We determined the concentration of carboxylated nanographene oxide (NGO-COOH) by fluorescence quenching experiments.Under the catalytic action of 1-(3-dimethylaminopropyl)-3-ethylcarbodiimide hydrochloride (EDC-HCl), PEG$(NH_2)_2$ was coupled with NGO-COOH through an amide reaction to obtain PEGylated nanomaterials. Then, F-TP and CXB were loaded onto the PEGylated nanomaterial through π-π and hydrogen bonding to synthesize the nano drug delivery system[33].Briefly, carboxylated NGO and bisaminated PEG were dissolved in deionized water at a concentration ratio of 1:4, sonicated for 1 h, and then EDC-HCl was added. The samples were stirred at room temperature for 24 h, centrifuged after dialysis, and freeze-dried to obtain NGO-PEG. NGO-PEG and F-TP were added to deionized water at a concentration ratio of 10:1 and stirred vigorously for 24 h at room temperature in the dark. NGO-PEG-FAP-targeting peptide (GPF) was obtained via centrifugation after dialysis. Next, CXB was added to the GPF solution; this mixture was sonicated and stirred at room temperature for 24 h. Unreacted CXB was removed via dialysis to obtain the CXB@NGO-PEG-FAP-targeting peptide(CGPF).

The NGO, NGO-PEG, GPF and CGPF were analyzed using a UV-Vis spectrophotometer (UV-3600, Shimadzu, Japan). The surface functional group changes were analyzed using Fourier transform infrared

spectroscopy (Tensor-27, Bruker, Germany). Data analysis was performed using Origin2019. Morphological characterization was performed using a JEOL JEM-2100F transmission electron microscope (JEOL Ltd., Japan). The hydrodynamic diameter profiles of NGO-COOH, NGO-PEG, GPF, and CGPF were obtained via dynamic light scattering (DLS) using Zetasizer Nano ZS90 (Malvern Omni-Optics, UK). The samples were prepared by solubilizing the nanoparticles in deionized water. Their zeta potentials were also measured using Nano ZS90 (Malvern Panalytical Ltd, UK).

Stability Test

To enhance the biocompatibility of NGOs, we modified them with PEG. The concentrations of NGO, NGO-PEG, and GPF in water- and serum-containing solutions were 1.0 mg/mL. We then assessed their stability by observing for the formation of precipitates during the 6 days of quiescence[34].

Fluorescence Recovery Experiment

Human dysplastic oral keratin-forming (DOK) cells were seeded in 6-well plates at a density of 1×10^6 cells/well. After 24 h of incubation, the original medium was replaced with a medium containing different concentrations of graphene-based GPF. The mixture was then incubated at 37℃ for 40 min. The NGO concentrations used were 0, 0.01, 0.02, 0.04, 0.08, and 0.1 mg/mL, sequentially. The cells were washed three times with low-temperature PBS after the final incubation, and 500 μL of PBS was added. The samples were filtered and analyzed using flow cytometry[35].

Drug Loading And In Vitro Release Assays

CXB/PBS solutions at 5, 10, 20, 30, 40, and 50 μg/mL were prepared, and PBS was placed in a cuvette as a blank control. The configured standard solutions were scanned using a UV spectrophotometer at 200–400 nm. The maximum absorption peak was found at a wavelength of 254 nm, and the absorbance values were recorded. The standard curve equation for CXB in PBS was obtained by plotting the concentration standard curve that was based on the relationship between the absorbance value at 254 nm and the concentration.

Then, 1 mg of GPF was added to 6 mL of PBS and the sample was sonicated to allow complete solubilization. Consequently, 1 mg of CXB was added and the sample was centrifuged after stirring at room temperature for 24 h. The centrifuged sample was dried in vacuum at 37℃ to obtain CGPF. The supernatant was diluted to a certain concentration, and the absorbance value was measured at 254 nm using a UV spectrophotometer. The actual concentrations were calculated by substituting the absorbance values into the linear regression equation, and the drug loading rate of GPF was calculated using **Eq. 1**.

Loading of celecoxib by nano-carriers: $LC=(M_0-M_1)/M$ (1)

Where LC is the drug loading capacity, M_0 is the initial drug mass (mg), M_1 is the drug mass in the supernatant (mg), and M is the mass of the nano-drug loading system (mg).

To study pH-dependent drug release, CGPF solutions were prepared in 1 ml of PBS at pH 7.4, pH 6.5 and pH 5.5 and shaken at 37℃ at 100 rpm. The concentration of released CXB was obtained at a predetermined time point by absorbance at 254 nm using UV-Vis spectroscopy. The precipitate was then centrifuged to recover the CGPF from the precipitate. drug release experiments were continued by resuspending the precipitate in PBS at pH 7.4, pH 6.5 and pH 5.5. We calculated the cumulative drug release according to **Eq. 2**[36].

Cumulative drug release (%) = Weight of released CXB (mg)/Weight of loaded CXB (mg) × 100 (2)

In Vitro Photothermal Analysis

The temperature changes of the NGO, NGO-PEG, GPF, CGPF, and PBS solutions after 5 min of 808-nm laser irradiation were monitored using infrared thermography (Ti400, Fluke, America). Temperature changes were also monitored for concentrations of 0.1, 0.2, 0.5, 1, and 2 mg/mL CGPF solutions and solutions at 0.5, 1, 1.5, and 2 W/cm^2 power, respectively. CGPF thermal stability was evaluated using five heating and cooling cycles.

Cell Culture

Human DOK and oral epithelial keratinocytes (HOK) were obtained from the European Collection of Authenticated Cell Cultures. Cells were cultured in 10% fetal bovine serum and 1% double antibody medium. Cells were cultured at 37℃ and 5% CO_2 in a humidified atmosphere. Cell digestion was performed with 0.25% EDTA, and passaging was to be and was performed within 3 days.

Cytotoxicity Assay

The CCK8 method was used to detect the toxicity of NGO, PEG, NGO-PEG, F-TP, GPF, free CXB, and CGPF in DOK and HOK cells. Cells were inoculated into 96-well plates at a density of 4000 cells/well for DOK and 6000 cells/well for HOK. The original medium was replaced with a fresh medium containing NGO, PEG, GP, F-TP, GPF, free CXB, and CGPF. The cells were then incubated for 24 h. Fresh medium (100 μL) containing 10% CCK8 was added, the cells were allowed to incubate in the solution for 40 min, and the absorbance was measured at 450 nm. The other group was incubated with different materials for 4 h, irradiated with NIR (808 nm, 1 W/cm^2) for 5 min, incubated for 20 h, and then incubated with 90 μL of a fresh medium containing 10 μL of CCK8 for 40 min. The absorbance was then measured at 450 nm.

We also used the CCK8 method to evaluate DOK cell viability under different pH conditions. Specifically, DOK cells were inoculated into 96-well plates at a density of 5000 cells/well, and after 24 h of incubation,

the original medium was replaced with a fresh medium containing CXB and CGPF at pH 7.4, 6.5, and 5.5. After 24 h of incubation, the medium was replaced with 90 μL of fresh medium containing 10 μL of CCK8, the samples were incubated for 40 min, and the absorbance was measured at 450 nm.

Cell Uptake Experiment

DOK cells were cultured at a density of 1×10^5 cells/well in laser confocal culture dishes and incubated for 24 h. The original medium was replaced with a fresh medium containing F-TP, GPF, and CGPF. The cells were then incubated for 4 h. The cells were washed three times with PBS and fixed using 4% paraformaldehyde. Cells were stained with DAPI (excitation, 488 nm) and then observed under an OLYMPUS FV1200 confocal laser-scanning microscope (Olympus, Osaka, Japan). HOK cells were used as FAP-negative controls and cultured in F-TP-containing medium to perform the above experiments and compare them with DOK cells.

The cells were additionally divided into F-TP, GPF, and CGPF groups. DOK cells were seeded into 24-well plates at a density of 1×10^5 cells/well and incubated overnight. The cells were incubated at 37℃ for 5, 15, 30, 60, and 120 min and rinsed three times with ice-cold PBS at each time point. The amount of fluorescence was analyzed using flow cytometry to assess cellular uptake.

In Vivo Fluorescence Imaging And In Vivo Treatment Of White Spots

Oral leukoplakia was induced in C57BL/6 mice (male, 6 weeks, 18–22 g) via oral administration of 4-nitroquinoline-1-oxide (4NQO)[37].Mice were freely drinking 100 μg/mL 4NQO aqueous solution protected from light and observed for OLK for 14–16 weeks.Four mice from each group underwent tissue collection following cervical dislocation at weeks 8, 12, and 16. The samples underwent hematoxylin and eosin (HE) staining to identify the modeling stage. After confirming successful modeling, we used FAP-targeted nanoprobes containing Cy5.5 for in vivo imaging using C57BL/6 mice with leukoplakia for in vivo biodistribution assays. Mice with leukoplakia were randomly divided into three groups and either CGPF, F-TP, or PBS was injected intraperitoneally following a dose of 31 mg/kg. Fluorescence signals were collected at different time intervals (2, 6, 8, and 24 h) after injection, using an *in vivo* imaging system (Xterme,Burker,America) to record the distribution of PBS, F-TP, and CGPF. The mice were executed 24 h after the injection, and the organs were harvested to observe drug metabolism in the heart, liver, spleen, lungs, and kidneys, using an imaging system.

Subsequently, the mice that had developed OLK were randomly divided into nine treatment groups, [1] CGPF, [2] CGPF + PTT, [3] CXB@NGO-PEG (CGP), [4] CGP + PTT, [5] GPF, [6] GPF + PTT, [7] CXB, [8] PBS + PTT, and [9] PBS, and with 4 mice in each group was intraperitoneally injected with the corresponding drug every 3 days for 4 weeks..The photothermal group of mice was irradiated with a 1 W/cm^2 laser for 5 min during the second and third week, at the leukoplakia lesion sites. The temperature rise of the laser treatment site was recorded using infrared thermography. Body weight and water consumption were

recorded every 2 days during the treatment period. Changes in the area and number of leukoplakia in mice were photographed and observed until the end of the experiment.

After the treatment, the mice were executed, and the tongues and major organs (heart, liver, spleen, lung, and kidney) underwent HE staining and immunohistochemistry analysis (FAP, KI67, and p53) to analyze the treatment effect and material safety.

For animal experiments, all animal procedures were performed in accordance with the standards of the National Regulations for the Care and Use of Laboratory Animals in China. Animal protocols were approved by the Animal Use and Care Committee of Shanxi Medical University (approval number: 2021 – 217, Taiyuan, China).

Statistical analysis

Statistical analysis was performed using Statistical Package for the Social Sciences software, and data are expressed as mean ± standard deviation (SD). Data analysis was performed using one-way analysis of variance. *$p < 0.05$, **$p < 0.01$, ***$p < 0.001$.

Results And Discussion

Immunohistochemical assay and cellular immunochemical assay to verify the high expression of FAP in OLK

FAP is a homodimeric integrative membrane gelatinase belonging to the serine protease family and is capable of cleaving the proline backbone of peptides and proteins[38, 39].Several studies have shown that FAP is expressed in tumor cells of epithelial origin like in breast, pancreatic, gastric, rectal, and cervical cancers, and OSCC, but not in normal adult tissues[40–42].Wang et al. showed that FAP downregulation inhibits cell proliferation and metastasis in OSCC, which suggests that FAP plays an important role in OSCC development[43].Numerous epidemiological and molecular biology studies have shown that inflammation significantly increases the risk of cancer[44].Progression from OLK to OSCC involves a complex inflammatory process[45]. Furthermore, Cai et al. showed that FAP expression is elevated in the tumor microenvironment and inflammatory settings[46].Based on the above, we hypothesized that FAP is highly expressed in OLK, and the sequencing results of Debodipta Das confirmed our conjecture that FAP is highly expressed in OLK. Next, we verify this result by experimental areas.

In the present study, we analyzed FAP expression levels in OLK and normal tissue sections via immunohistochemistry, and OLK tissues showed higher FAP expression than normal oral mucosa tissues. Notably, FAP was located in the epithelial layer and part of the mesenchyme of OLK tissue and localized mainly in the cytoplasm (Fig. 1a and b). The FAP expression levels in DOK cells and HOK normal cells were analyzed by cellular immunochemistry ,and DOK cells showed higher FAP expression

than HOK cells, with FAP located in the cytoplasm of DOK cells (Fig. 1c and d). These results suggest that FAP is highly expressed in OLK.

Synthesis And Characterization Of Cgpf

To synthesize CGPF, PEGylated NGO was synthesized by modifying the NGO with PEG by following the prevailing method in the literature. Subsequently, the NGO-PEG was bound to the peptide chain with a fluorophore attached, and CXB was added to construct a nano-drug delivery system. On exposure to UV rays, NGO had a maximum absorption peak at 230 nm, which is the characteristic absorption peak of C = O. After modifying with PEG, the NGO-PEG had a maximum absorption peak at 240 nm owing to the reduction of NGO by PEG through an amide reaction, which shifted the absorption peak to the right. The F-TP had a clear UV absorption peak at 495 nm, and the GPF showed the characteristic F-TP peak at 495 nm, indicating the successful binding of F-TP to NGO-PEG. There were clear absorption peaks at 254 nm for both CXB and CGPF. Therefore, CXB can be considered to have successfully bound to GPF (Fig. 2a).

In addition, we characterized the probe using FTIR spectroscopy (Fig. 2b). NGO-PEG had a C-O-C stretching vibration peak at 946 cm^{-1}, C-N stretching vibration peak at 1103 cm^{-1}, and C = O stretching vibration peak in the amide bond region at 1511 cm^{-1}. This indicates that the NGO -COOH group underwent an amide reaction with the terminal amino group of $PEG(NH_2)_2$. New peaks were observed at 1251 cm^{-1}. These changes in the chemical bonding vibrational peaks confirm that NGO-PEG formed bonds with F-TP through hydrogen and π–π bond interactions. The 1243cm^{-1},2765$cm^{-1}$and 3606cm^{-1} peaks were caused by benzene rings and other functional groups indicating that the nano-drug delivery system was successfully fabricated.

Zeta potential analysis was performed to verify NGO modification by PEG and the loading of F-TP and CXB. The negative potential of NGO-PEG (-22 mV) was lower than that of NGO (-27.3 mV) owing to the reaction between the negative NGO carboxyl group and the PEG amino group. The zeta potential reduced to -21 mV upon attachment of the FAP-targeting peptide and to -20.4 upon CXB attachment (Fig. 2c). The change in potential indicates the successful synthesis of the nano-drug delivery system.

The morphologies of the studied nanoparticles (NGO, NGO-PEG, GPF, and CGPF) were investigated using transmission electron microscopy (Fig. 2d). Notably, the thin and transparent NGO sheets had a relatively large and smooth surface. After polyethylene glycolization, the nano-sheet surfaces appeared corrugated that facilitated functionalization of the nanoparticles with drugs or other bioactive molecules. After loading F-TP and CXB, the NGO-PEG sheet layers had different shapes.

The NGO, NGO-PEG, GPF, and CGPF hydrated particle sizes were determined using DLS. The particles were 345.6, 122.7, 140.5, and 179.5 nm in diameter, respectively indicating that the NGO particle size was effectively reduced following PEG modification. Furthermore, the particle size increased following FAP-targeting peptide and CXB attachment. In addition, the particle size reduced after polyethylene

glycolization, as the size range of NGO particles was 295–459 nm, while that of NGO-PEG particles was 106–142 nm (Fig. 2e).

Stability Experiments

Because of poor hydrophilicity of NGO, we used PEG to enhance its stability. As shown in Fig. 2f, in PBS containing NGO, a clear precipitate was observed after 1 day of resting (f-). In contrast, NGO-PEG and CGPF were uniformly dispersed in PBS and were stable even after 6 days (f-). To simulate the blood environment in vivo, we examined nanocomposite stability in 10% FBS. As shown in Fig. 2f, a large amount of precipitate was observed in 10% FBS containing NGO after 1 day (f-). In contrast to NGO, NGO-PEG and CGPF remained stably dispersed in 10% FBS without precipitation(f-).

Fluorescence Quenching And Recovery

The excitation wavelength of FITC is 495 nm, and the fluorescence quenching experiment showed that when the concentration of NGO was 0.1 mg/mL, the peak fluorescence absorption of FITC dropped to 0. This indicates that 0.1 mg/mL of NGO can quench the fluorescence coupled to 10 μg/mL of the FAP target peptide (Fig. 3a). To investigate if FITC can dislodge from the NGO carrier to restore florescence upon encountering the target molecule and thus act as a fluorescence “switch,” we analyzed the recovery of fluorescence intensity after incubation of GPF containing different concentrations of NGO with DOK cells for 40 min by flow cytometry.As shown in Fig. 3b, despite the strong fluorescence quenching effect of 0.1 mg/mL NGO, equal amounts of fluorescence were detected in all five experimental groups when compared with that in the control group. The amount of fluorescence detected in the experimental group was close to that in the control group. Taken together, these results indicate that FITC can shed from GPF to localize to OLK after the probe encounters the target molecule FAP.

Drug Loading And Release Experiments

The UV-Vis absorbance of CXB was measured at 254 nm, and the standard curve was plotted (Fig. 3c). The linear regression equation of CXB was:

$A = 0.02683C + 0.09927$ ($R^2 = 0.98156$),

where A is the UV-Vis absorbance of CXB at 254 nm and C is the concentration of CXB (μg/mL), and $R^2 = 0.98156$ indicates a good linear relationship and plausible standard curve. The corresponding CXB concentration was derived from the above linear regression equation, and the drug loading rate of the nano-targeted probe was calculated as 38.82% according to Eq. 1.

Owing to the difference in the microenvironments between inflammatory and normal tissues, we set up different pH values to simulate each tissue. The drug release properties of the nano-delivery system were

evaluated in PBS solutions at pH 7.4, 6.5 and 5.5.The CXB release profiles from the nano-drug-loaded system at different pH values are shown in Fig. 3d. CXB exhibited a sustained *in vitro* release from the nano-carrier system and showed some degree of pH sensitivity. The amount and rate of drug release at pH 5.5 was the highest followed by that at pH 6.5 and pH 7.4, at the same time interval. The nano-carrier system eventually released 65.02% and 81.96% of CXB at pH 6.5 and 5.5, respectively, but at pH 7.4, only 51.47% was released. Taken together, these results suggest that the nano-drug delivery system is pH-sensitive and can selectively release CXB. The results of this experiment suggest that our constructed CGPF is sufficiently stable to prevent it from releasing the drug before it reaches the lesion site.Our results are in good agreement with those of previous studies describing similar pH-responsive drug-release behaviors[47].

In Vitro Photothermal Effect

Figure 4 In vitro photothermal effect. (a) Photothermal profile images of PBS, NGO, NGO-PEG, GPF, and CGPF under 808 nm radiation. (b) Photothermal profile images of CGPF aqueous solution with different concentrations under 808 nm radiation. (c) Photothermal profile images of CGPF aqueous solution with different power under 808 nm radiation. (d) Photothermal performance of CGPF over five laser on/off cycles

Prior studies have shown that graphene oxides exhibit a photothermal effect and can convert absorbed light energy into heat energy under near-infrared light irradiation, resulting in an increase in the temperature of the surrounding environment. To determine whether NGO-PEG also has a photothermal therapeutic effect, near-infrared light (808 nm, 1.0 W/cm^2) was used to irradiate the NGO, NGO-PEG, GPF, and CGPF solutions, while PBS was used as a control. As shown in Fig. 4a, the NGO, NGO-PEG, GPF, and CGPF solutions warmed rapidly under laser irradiation, while PBS showed essentially no significant warming. The temperature of the CGPF solution increased sharply with increasing time and concentration (Fig. 4b). At the same concentration, the temperature of the CGPF solution increased with increasing power of irradiation (Fig. 4c). The infrared (IR) thermal images confirmed similar results. Notably, no significant decay was detected in the temperature increase after five heating and cooling cycles, indicating excellent photothermal stability (Fig. 4d). These results indicate that GO modification by PEG does not destroy the photothermal effect of the material itself. Owing to the effective restoration of π–π conjugation via chemical reduction, the energy absorbed by the reduced GO nanomaterials can be rapidly converted to higher thermal energy. The GO photothermal performance improved after modification by PEG, and the radiothermal effect of CGPF under irradiation with near-infrared light caused a significant increase in the temperature of the surrounding environment, which is of great significance for the photothermal treatment of white spots.

In Vitro Cytotoxicity

Prior to *in vitro* evaluation of the synergistic therapeutic properties of CGPF, its cytotoxicity and therapeutic feasibility were investigated using standard CCK8 assays. The cytotoxicity of NGO, PEG, NGO-PEG, F-TP, GPF, CXB, and CGPF in DOK and HOK cells was assessed. Twenty-four hours post-treatment, we observed that in the concentration range studied, NGO-PEG exhibited lower cytotoxicity than NGO in DOK and HOK cells, and NGO-PEG and GPF had no significant effect on DOK and HOK cell proliferation. In addition, we found that cell viability of the CGPF group was significantly lower than that of the NGO-PEG and GPF groups. However, cell viability was higher in the CGPF group than in the free CXB group at the same CXB concentration. The toxicity of free CXB in DOK cells was much higher than that in HOK cells (Fig. 5a). Under photothermal conditions, the cell viability of the NGO, NGO-PEG, GPF, and CGPF groups decreased relative to that of the non-photothermal group, especially the CGPF group, which showed a significant decrease in cell viability (Fig. 5b). This can be explained as follows: (1) NIR radiation kills DOK cells and promotes cell membrane permeability and increases nanomaterial internalization, accelerating drug release in DOK cells and enhancing medication effects; (2) NIR laser-assisted thermal therapy destroys drug-resistant DOK cells and helps promote accumulation of CXB in the nucleus, thereby improving medication efficacy. In addition, cell viability of the CGPF group was much higher than that of the free CXB group for the same CXB concentration, which may be explained by the incomplete release of CXB at pH = 7.4.

Subsequently, DOK cell viability tests were performed under different pH conditions, and the results are shown in Fig. 5c. The cell viability of the control and CXB groups did not change significantly at different pH values, whereas the viability of the CGPF group decreased with the pH of the culture medium. This further suggests that the pH of the culture environment affects drug release and thus cell viability and that the acidic pH of the inflammatory environment surrounding the leukoplakia tissue limits the effective release range of our drugs and reduces their toxicity to normal cells and tissues.

Cellular Uptake Experiments

To verify the targeting of F-TP, the FAP-responsive properties of CGPF at the cellular level, and whether the nanoparticles could be effectively administered, laser confocal scanning microscopy experiments were performed to assess the uptake of the F-TP, GPF, and CGPF in DOK and HOK cells. Blue fluorescence (excitation, 460 nm) was used to identify the nuclei of DOK and HOK cells, while the red channel (excitation, 490 nm) represents the FITC fluorescence signal. As shown in Fig. 5e, the FITC fluorescent signal colocalized to the red signal. F-TP were observed on the cell membrane and cytoplasm of DOK cells, consistent with the FAP expression profile. In the negative control, no red fluorescence signal was observed in HOK cells. In summary, the F-TP, GPF, and CGPF showed high binding to FAP expressed in DOK, which could be taken up by DOK cells, and the FAP-specific peptide on CGPF was cleaved to activate FITC.

Additional time-dependent assays of the F-TP, GPF, and CGPF were performed using DOK cells. The results showed that the uptake of the F-TP, GPF, and CGPF by DOK cells was time-dependent. The cellular

uptake of the F-TP and GPF did not differ significantly, indicating that NGO had no effect on F-TP uptake. Cell uptake rates in F-TP and GPF groups were 82.235% and 83.77% at 30 min and 85.08% and 83.9% 120 min, respectively. The cellular uptake rate of CGPF was 80.22% at 30 min; at 120 min, it decreased to 64.85% (Fig. 5d). This is owing to the decrease in the uptake rate as a result of cell death due to drug release after the nano-drug delivery system was internalized into the cells.

Successful Establishment Of A Mouse Olk Model

4NQO is an aromatic amine heterocyclic compound that is extensively recognized as a chemical precursor carcinogen[48].Studies have shown that 4NQO can help develop pre-cancerous or cancer models by inducing intracellular oxidative stress, DNA endocytosis, mutagenesis, and tumor initiation[49, 50].The 4NQO-induced pre-cancerous lesion model has a multi-stage dynamic continuum, from normal oral mucosa to OLK to OSCC, with pathological stages that undergo hyperplasia, heterogeneous hyperplasia (mild, moderate, and severe), carcinoma in situ, and invasive squamous cell carcinoma[51].This model closely mimics the heterogeneous oncogenic proliferation process in the human oral cavity and is suitable for studying the specific OLK oncogenic process for the development of biomarkers for early detection and epithelial cell transformation[52, 53].After 100 μg/mL 4NQO was administered via drinking water, all mice were anesthetized by injection of chloral hydrate at 8, 12, and 16 weeks[54].We observed the 4NQO-induced changes by pulling the tongues outward and selected the typical tissues for histopathological examination. At week 8, the mice had mild atrophy of the tongue papillae and a smooth white dorsum of the tongue, and HE staining showed a mild or normal heterogeneous lesion phenotype. At week 12, the dorsum of the tongue was rough and smooth, white plaque-like lesions appeared on the tongue tissue, and HE staining showed mild or moderate heterogeneous hyperplasia. Thereafter, all mice gradually developed inseparable white plaques. At week 16, they developed typical lesions similar to those in human OLK (Fig. 6). 4NQO has been shown to cause cancer in different sites of the oral cavity such as the dorsum of the tongue, ventral part of the tongue, palate, and esophagus. Many researchers have shown that lesions of the tongue occur almost 100% of the time, particularly in the dorsal mucosa of the tongue. In the present study, lesions were predominantly located on the dorsum of the tongue, with a few lesions located on the floor of the mouth or along the lateral edge of the tongue, which is consistent with previous reports. These findings indicate the successful establishment of an OLK mouse model, with no significant damage to the major organs by 4NQO, which can be used for further *in vivo* experiments.

In Vivo Biodistribution

Precise localization and optimal timing are essential for the successful synergistic treatment of leukoplakia. To assess the ability of FAP to activate fluorescence in vivo, F-TP and CGPF were injected intraperitoneally into mice, and the PBS group was used as a control. As shown, the activatable CGPF fluoresced rapidly and specifically at the white spots within 8 h, which helped distinguish the white areas from normal tissue. Interestingly, no detectable fluorescence was found in any other area without

leukoplakia lesions owing to the initial fluorescence quenching of CGPF. Thereafter, the images showed gradual enhancement of FL signal in both F-TP-injected and CGPF-injected mice in the leukoplakic areas and reached a maximum 8 h post-injection. In contrast, no FL signal was observed in the control group 24 h after the PBS injection. This suggests that the F-TP and CGPF can be effectively delivered to white spots and that CGPF can be specifically activated by FAP. Subsequent in vitro FL imaging of the excised tongues and major organs of F-TP and CGPF-treated mice after 24 h clearly showed that fluorescence activation was visible at the white spot of the excised tongue and had a superior FL signal than the major organs (Fig. 7a). Notably, a weaker fluorescent signal was present in the isolated liver than in other organs, reflecting the major hepatic clearance process of F-TP and CGPF.

In Vivo Targeting And Photothermal Effects

Encouraged by the activatable NIR fluorescence imaging data, we next explored the feasibility of CGPF for NIR PTT in vivo, and the results provided the correct time point and location specificity for laser irradiation. CGPF and PBS were injected intraperitoneally into mice with white plaque lesions, and infrared thermography and temperature changes at the tumor site were monitored 5 min after NIR irradiation. Considering the threshold temperature for PTT (43°C), the high temperature of CGPF 8 h after administration far exceeded the requirement for thermotherapy to achieve an optimal photothermal treatment effect. Notably, lesion temperatures in the 6- and 24-h post-injection groups showed lower maximums than those in the 8-h post-injection groups owing to insufficient accumulation in the leukoplakic lesion sites. In contrast, PBS-treated mice showed only slight warming (Fig. 7b). With photothermal imaging guidance, we selected 8 h after injection as the appropriate time for synergistic treatment. Figure 7c and d show that the temperature of the oral white-spot site of mice irradiated with NIR for 5 min after 8 h of GPF and CGPF injection increased significantly, while the temperature of mice injected with PBS and CGP did not change significantly after irradiation. This is because PBS has no photothermal effect and CGP had a photothermal effect; however, the absence of F-TP prevented it from aggregating at the oral white-spot site in the mice.

In Vivo Therapeutic Effect And Safety Assessment Of Olk

To evaluate the *in vivo* therapeutic performance of CGPF in OLK, we selected 45 mice with typical white plaque lesions on the dorsal surface of the tongue and randomly divided them into nine groups (n = 5) for different treatments, with PBS-injected mice as negative controls. Changes in white plaques of the tongue were continuously monitored and recorded in each group for 1 month after the different treatments. Impressive leukoplakia suppression was achieved within 1 month after CGPF combined with 808-nm laser treatment, but not in the other groups, indicating that chemotherapy in synergy with PTT achieved better therapeutic effects than chemotherapy alone (Fig. 8a).

Interestingly, the CGPF + laser group showed almost complete eradication during the treatment period without any recurrence. In contrast, the CGPF and GPF + laser groups showed limited cancer suppression

with partial improvement, indicating that neither drug treatment alone (CGPF) nor targeted material alone combined with laser treatment (GPF + laser) could achieve superior results than the targeted material delivery system combined with photothermal treatment (CGPF + laser). This may be owing to the graphene oxide structure, which allows CXB to make full contact with the lesion site. In the presence of the F-TP, the material and drug can accurately and rapidly reach the OLK lesion site with high FAP expression. This is similar to the specific recognition and binding of antigens to antibodies. Furthermore, when the CGPF successfully reached the lesion and achieved significant aggregation, excellent photothermal properties of NGO allowed laser irritation to rapidly warm the lesion, and when the photothermal temperature reached approximately 50℃, the lesion area experienced a significant effect. This explains why the treatment effect of CGPF + laser was better than that of CGPF or GPF + laser, while anisotropic hyperplasia in the CGP, CGP + laser, and CXB groups continued to deteriorate. We consider that in the absence of targeted peptides, the material delivery system or the drug alone cannot reach the lesion accurately and quickly, and only a small amount of the drug can work at the lesion after it is injected intraperitoneally into the systemic circulation, so the effect of the laser becomes very weak in these treatment groups. While the cancer in the GPF, PBS, and laser groups progressed, which again proved that the material or laser alone could not exert any therapeutic effect.

In summary, even though the targeted nano-delivery system achieved specific binding of the targeted peptide to the lesion site FAP, improving the contact area of the drug will provide better therapeutic effects,the treatment effect of CGPF alone was limited. In contrast,the targeting of CGPF provided good combined photothermal chemotherapy for the treatment of OLK, and the CGPF + laser treatment group achieve better results; its therapeutic effects were superior to those of CGPF, and it effectively inhibited the malignant development of OLK.

In addition, we did not use local injection in the experiment but used intraperitoneal injection for the following reasons: first, the local drug delivery method will be affected by factors such as saliva secretion and tongue movement, which will make the operation more difficult, and the stimulated saliva secretion will dilute the drug and eventually affect the therapeutic effect. Secondly, the number of injections will cause damage to the tongue and affect feeding, which further affects the efficacy of the drug. Thirdly, the injection itself is one of the stimulating factors, which may induce or aggravate the leukoplakia lesion, and the result has certain influence. Then again, our experiment successfully proved that the oral leukoplakia in mice was cured by intraperitoneal injection of CGPF, which indicates that our nano-targeting system CGPF has a good targeting effect and can make it gather well in the oral leukoplakia lesions to achieve the ideal treatment effect.

In addition to therapeutic effects, long-term safety of the material must be considered. Mitigating drug biotoxicity is essential for biomedical applications. Therefore, we investigated the biocompatibility of different materials using C57BL/6 mice. We continuously monitored and recorded weight changes in the mice during treatment. Notably, negligible body weight fluctuations were observed during treatment (Fig. 8b), and the material exhibited superior biosafety. To further confirm the treatment effect, tongue leukoplakia tissue was dissected at the end of treatment, and pathological changes were assessed

through histological and immunohistochemical analyses. As shown in Fig. 8c, significant leukoplakia cell damage and diminished or absent anisotropic proliferation were observed in the CGPF + laser group, and partial leukoplakia cell damage and diminished anisotropic proliferation were observed in the CGPF and GPF + laser groups. In contrast, enhanced heterogeneous hyperplasia and cancerous lesions were observed in the CGP, CGP + laser, CXB, GPF, PBS, and laser groups. In addition, the experimental results showed that the expression of FAP, KI67 and p53 was highest in the control group, compared to a significant downregulation of FAP, KI67 and p53 expression after treatment with CGPF + laser. (Fig. 8d).

As expected, HE staining of the major organs (heart, liver, spleen, lung, and kidney) showed no significant histopathological damage or inflammation in any group (Fig. 8e). These results suggest that our targeted nano-drug delivery system combined with PTT significantly improved the therapeutic efficacy of OLK with a good biosafety profile.

Conclusion

We successfully validated the high expression of FAP in oral leukoplakia and constructed a novel nano-drug delivery system CGPF targeting FAP for combined drug and photothermal treatment of OLK. The system can target OLK tissues with high FAP expression and be specifically cleaved by FAP, thus activating fluorescence and achieving precise localization at the leukoplakia lesion site. In addition, CXB is slowly released from the nano-drug delivery system in the acidic inflammatory environment of leukoplakia tissues, enabling local targeted drug therapy and effectively improving efficacy. the superior photothermal properties of NGO-PEG allow CGPF to be used in combination with PTT. Our in vivo and in vitro studies have shown that CGPF can be specifically targeted to OLK-affected areas for NIR PTT. based on the precise localization of FAP-targeted peptides to leukoplakia lesions, we have successfully achieved better and more comprehensive therapeutic results by combining drug therapy with photothermal treatment at the targeted sites. Our study provides an excellent approach for synergistic drug therapy and photothermal treatment of OLK, which facilitates a more complete treatment of leukoplakia and blocks its cancerous process with good therapeutic effects, which may open up new opportunities for its treatment for more promising clinical applications.

Declarations

Author contribution R.L. and Y. Z. contributed equally to this work. R.L.: Validation,Writing – review & editing, Supervision , Conceptualization, Project administration, Funding acquisition.Y.Z.: Data curation, Methodology, Formal analysis, Investigation,Writing – original draft, Visualizatio. T. L.:Methodology, Resources, Writing – review & editing. Y. L.: Writing – review & editing.C.W.: Resources, Writing – review & editing. R.G.:Validation, Writing – review & editing. Chen Liu: Resources.X.L.: Conceptualization. B.L.: Conceptualization.

Funding This study was supported by Shanxi Province Basic Research Program (20210302123311) ,Research Project Supported by Shanxi Scholarship Council of China(2021-087), Fund Program for the

Scientific Activities of Selected Returned Overseas Professionals in Shanxi Province(20220020), Teaching Reform and Innovation Programs of Higher Education Institutions in Shanxi (J20220404), Science and Technology Innovation Leader and Key Talent Team Project of Shanxi Province (202204051002034) and 2022 Innovation Project of Postgradute Education in Shanxi Province(Master).

Data availability Any data or material that support the fndings of this study can be made available by the corresponding author upon request.

Materials availability Any data or material that support the fndings of this study can be made available by the corresponding author upon request.

Ethics approval and consent to participate All institutional and national guidelines for the care and use of laboratory animals were followed. All human OLK and NOM samples were obtained and used under informed written patient consent and local ethical committee approval.

Consent for publication All the authors provided consent for publication.

Competing interests The authors declare no competing interests.

References

1. van der Waal I. Historical perspective and nomenclature of potentially malignant or potentially premalignant oral epithelial lesions with emphasis on leukoplakia-some suggestions for modifications. Oral Surg Oral Med Oral Pathol Oral Radiol. 2018;125(6):577-81.
2. Ding T, Zou J, Qi J, et al. Mucoadhesive Nucleoside-Based Hydrogel Delays Oral Leukoplakia Canceration. J Dent Res. 2022;101(8):921-30.
3. Holmstrup P, Vedtofte P, Reibel J, et al. Oral premalignant lesions: is a biopsy reliable? J Oral Pathol Med. 2007;36(5):262-6.
4. Kerr A R, Lodi G. Management of oral potentially malignant disorders. Oral Dis. 2021;27(8):2008-25.
5. Annaji M, Poudel I, Boddu S H S, et al. Resveratrol-loaded nanomedicines for cancer applications. Cancer Rep (Hoboken). 2021;4(3):e1353.

6. Zhao M, Jing Z, Zhou L, et al. Pharmacokinetic Research Progress of Anti-tumor Drugs Targeting for Pulmonary Administration. Curr Drug Metab. 2020;21(14):1117-26.
7. Zhang H, Li Y, Pan Z, et al. Multifunctional Nanosystem Based on Graphene Oxide for Synergistic Multistage Tumor-Targeting and Combined Chemo-Photothermal Therapy. Mol Pharm. 2019;16(5):1982-98.
8. Cheng Y, Weng S, Yu L, et al. The Role of Hyperthermia in the Multidisciplinary Treatment of Malignant Tumors. Integr Cancer Ther. 2019;18:1534735419876345.
9. Lin L, Song C, Wei Z, et al. Multifunctional photodynamic/photothermal nano-agents for the treatment of oral leukoplakia. J Nanobiotechnology. 2022;20(1):106.
10. Zhao L, Chen J, Pang Y, et al. Fibroblast activation protein-based theranostics in cancer research: A state-of-the-art review. Theranostics. 2022;12(4):1557-69.
11. Dendl K, Koerber S A, Kratochwil C, et al. FAP and FAPI-PET/CT in Malignant and Non-Malignant Diseases: A Perfect Symbiosis? Cancers (Basel). 2021;13(19).
12. Fitzgerald A A, Weiner L M. The role of fibroblast activation protein in health and malignancy. Cancer Metastasis Rev. 2020;39(3):783-803.
13. Givel A M, Kieffer Y, Scholer-Dahirel A, et al. miR200-regulated CXCL12β promotes fibroblast heterogeneity and immunosuppression in ovarian cancers. Nat Commun. 2018;9(1):1056.
14. Keane F M, Yao T W, Seelk S, et al. Quantitation of fibroblast activation protein (FAP)-specific protease activity in mouse, baboon and human fluids and organs. FEBS Open Bio. 2013;4:43-54.
15. Linz C, Brands R C, Kertels O, et al. Targeting fibroblast activation protein in newly diagnosed squamous cell carcinoma of the oral cavity - initial experience and comparison to [(18)F]FDG PET/CT and MRI. Eur J Nucl Med Mol Imaging. 2021;48(12):3951-60.
16. Xi C R, Di Fazio A, Nadvi N A, et al. An improved production and purification protocol for recombinant soluble human fibroblast activation protein alpha. Protein Expr Purif. 2021;181:105833.
17. Sun Y, Liu N, Guan X, et al. Immunosuppression Induced by Chronic Inflammation and the Progression to Oral Squamous Cell Carcinoma. Mediators Inflamm. 2016;2016:5715719.
18. Das D, Maitra A, Panda C K, et al. Genes and pathways monotonically dysregulated during progression from normal through leukoplakia to gingivo-buccal oral cancer. NPJ Genom Med. 2021;6(1):32.
19. de Melo-Diogo D, Lima-Sousa R, Alves C G, et al. Graphene family nanomaterials for application in cancer combination photothermal therapy. Biomater Sci. 2019;7(9):3534-51.
20. Jiang B P, Zhou B, Lin Z, et al. Recent Advances in Carbon Nanomaterials for Cancer Phototherapy. Chemistry. 2019;25(16):3993-4004.
21. Ma K, Fu D, Liu Y, et al. Cancer cell targeting, controlled drug release and intracellular fate of biomimetic membrane-encapsulated drug-loaded nano-graphene oxide nanohybrids. J Mater Chem B. 2018;6(31):5080-90.

22. Mo Y, Liu W, Liu P, et al. Multifunctional Graphene Oxide Nanodelivery Platform for Breast Cancer Treatment. Int J Nanomedicine. 2022;17:6413-25.
23. Mousavi S M, Hashemi S A, Ghasemi Y, et al. Applications of graphene oxide in case of nanomedicines and nanocarriers for biomolecules: review study. Drug Metab Rev. 2019;51(1):12-41.
24. Wang K, Ruan J, Song H, et al. Biocompatibility of Graphene Oxide. Nanoscale research letters. 2011;6(1):8-.
25. Ding Y F, Kwong C H T, Li S, et al. Supramolecular nanomedicine derived from cucurbit[7]uril-conjugated nano-graphene oxide for multi-modality cancer therapy. Biomater Sci. 2021;9(10):3804-13.
26. Guo S, Nishina Y, Bianco A, et al. A Flexible Method for Covalent Double Functionalization of Graphene Oxide. Angew Chem Int Ed Engl. 2020;59(4):1542-7.
27. Lombardi L, Kovtun A, Mantovani S, et al. Visible-Light Assisted Covalent Surface Functionalization of Reduced Graphene Oxide Nanosheets with Arylazo Sulfones. Chemistry. 2022;28(26):e202200333.
28. Vacchi I A, Guo S, Raya J, et al. Strategies for the Controlled Covalent Double Functionalization of Graphene Oxide. Chemistry. 2020;26(29):6591-8.
29. Daniyal M, Liu B, Wang W. Comprehensive Review on Graphene Oxide for Use in Drug Delivery System. Curr Med Chem. 2020;27(22):3665-85.
30. Mirrahimi M, Alamzadeh Z, Beik J, et al. A 2D nanotheranostic platform based on graphene oxide and phase-change materials for bimodal CT/MR imaging, NIR-activated drug release, and synergistic thermo-chemotherapy. Nanotheranostics. 2022;6(4):350-64.
31. Sugumaran P J, Liu X L, Herng T S, et al. GO-Functionalized Large Magnetic Iron Oxide Nanoparticles with Enhanced Colloidal Stability and Hyperthermia Performance. ACS Appl Mater Interfaces. 2019;11(25):22703-13.
32. Guo W, Chen Z, Feng X, et al. Graphene oxide (GO)-based nanosheets with combined chemo/photothermal/photodynamic therapy to overcome gastric cancer (GC) paclitaxel resistance by reducing mitochondria-derived adenosine-triphosphate (ATP). J Nanobiotechnology. 2021;19(1):146.
33. Wang L, Yu D, Dai R, et al. PEGylated doxorubicin cloaked nano-graphene oxide for dual-responsive photochemical therapy. International Journal of Pharmaceutics. 2019;557:66-73.
34. Li R, Wang Y, Du J, et al. Graphene oxide loaded with tumor-targeted peptide and anti-cancer drugs for cancer target therapy. Scientific reports. 2021;11(1):1725-.
35. Li R, Gao R, Wang Y, et al. Gastrin releasing peptide receptor targeted nano-graphene oxide for near-infrared fluorescence imaging of oral squamous cell carcinoma. Scientific reports. 2020;10(1):11434-.
36. Dash B S, Lu Y-J, Chen H-A, et al. Magnetic and GRPR-targeted reduced graphene oxide/doxorubicin nanocomposite for dual-targeted chemo-photothermal cancer therapy. Materials Science and Engineering: C. 2021;128:112311.

37. Wang C, Niu W, Chen H, et al. Nicotine suppresses apoptosis by regulating α7nAChR/Prx1 axis in oral precancerous lesions. Oncotarget. 2017.
38. Fitzgerald A A, Weiner L M. The role of fibroblast activation protein in health and malignancy. Cancer Metastasis Rev. 2020;39(3):783-803.
39. Jiang G-M, Xu W, Du J, et al. The application of the fibroblast activation protein α-targeted immunotherapy strategy. Oncotarget. 2016;7(22):33472-82.
40. Garin-Chesa P, Old L J, Rettig W J. Cell surface glycoprotein of reactive stromal fibroblasts as a potential antibody target in human epithelial cancers. Proceedings of the National Academy of Sciences of the United States of America. 1990;87(18):7235-9.
41. Ren J, Smid M, Iaria J, et al. Cancer-associated fibroblast-derived Gremlin 1 promotes breast cancer progression. Breast cancer research : BCR. 2019;21(1):109-.
42. Dourado R C, Porto L P A, Leitão Á C G H, et al. Immunohistochemical Characterization of Cancer-associated Fibroblasts in Oral Squamous Cell Carcinoma. Applied Immunohistochemistry & Molecular Morphology. 2018;26(9).
43. Wang Y, Jing Y, Ding L, et al. Epiregulin reprograms cancer-associated fibroblasts and facilitates oral squamous cell carcinoma invasion via JAK2-STAT3 pathway. Journal of experimental & clinical cancer research : CR. 2019;38(1):274-.
44. Crusz S M, Balkwill F R. Inflammation and cancer: advances and new agents. Nature Reviews Clinical Oncology. 2015;12(10):584-96.
45. Sun Y, Liu N, Guan X, et al. Immunosuppression Induced by Chronic Inflammation and the Progression to Oral Squamous Cell Carcinoma. Mediators Inflamm. 2016;2016:5715719-.
46. Zi F, He J, He D, et al. Fibroblast activation protein α in tumor microenvironment: recent progression and implications (review). Molecular medicine reports. 2015;11(5):3203-11.
47. Yang X, Zhang X, Ma Y, et al. Superparamagnetic graphene oxide–Fe3O4nanoparticles hybrid for controlled targeted drug carriers. Journal of Materials Chemistry. 2009;19(18):2710-4.
48. Chen Q, Dan H, Tang F, et al. Photodynamic therapy guidelines for the management of oral leucoplakia. Int J Oral Sci. 2019;11(2):14-.
49. Li Q, Dong H, Yang G, et al. Mouse Tumor-Bearing Models as Preclinical Study Platforms for Oral Squamous Cell Carcinoma. Frontiers in oncology. 2020;10:212-.
50. Barcessat A R R, Huang I, Rabelo G D, et al. Systemic toxic effects during early phases of topical 4-NQO-induced oral carcinogenesis in rats. Journal of Oral Pathology & Medicine. 2014;43(10):770-7.
51. Vered M, Yarom N, Dayan D. 4NQO oral carcinogenesis: animal models, molecular markers and future expectations. Oral Oncology. 2005;41(4):337-9.
52. Kong X, Yang X, Zhou J, et al. Analysis of plasma metabolic biomarkers in the development of 4-nitroquinoline-1-oxide-induced oral carcinogenesis in rats. Oncol Lett. 2015;9(1):283-9.
53. Ludwig S, Hong C-S, Razzo B M, et al. Impact of combination immunochemotherapies on progression of 4NQO-induced murine oral squamous cell carcinoma. Cancer Immunology,

Immunotherapy. 2019;68(7):1133-41.
54. Gumus R, Capik O, Gundogdu B, et al. Low vitamin D and high cholesterol facilitate oral carcinogenesis in 4NQO-induced rat models via regulating glycolysis. Oral Dis. 2021.

Scheme 1

Scheme 1 is available in Supplementary Files section.

Figures

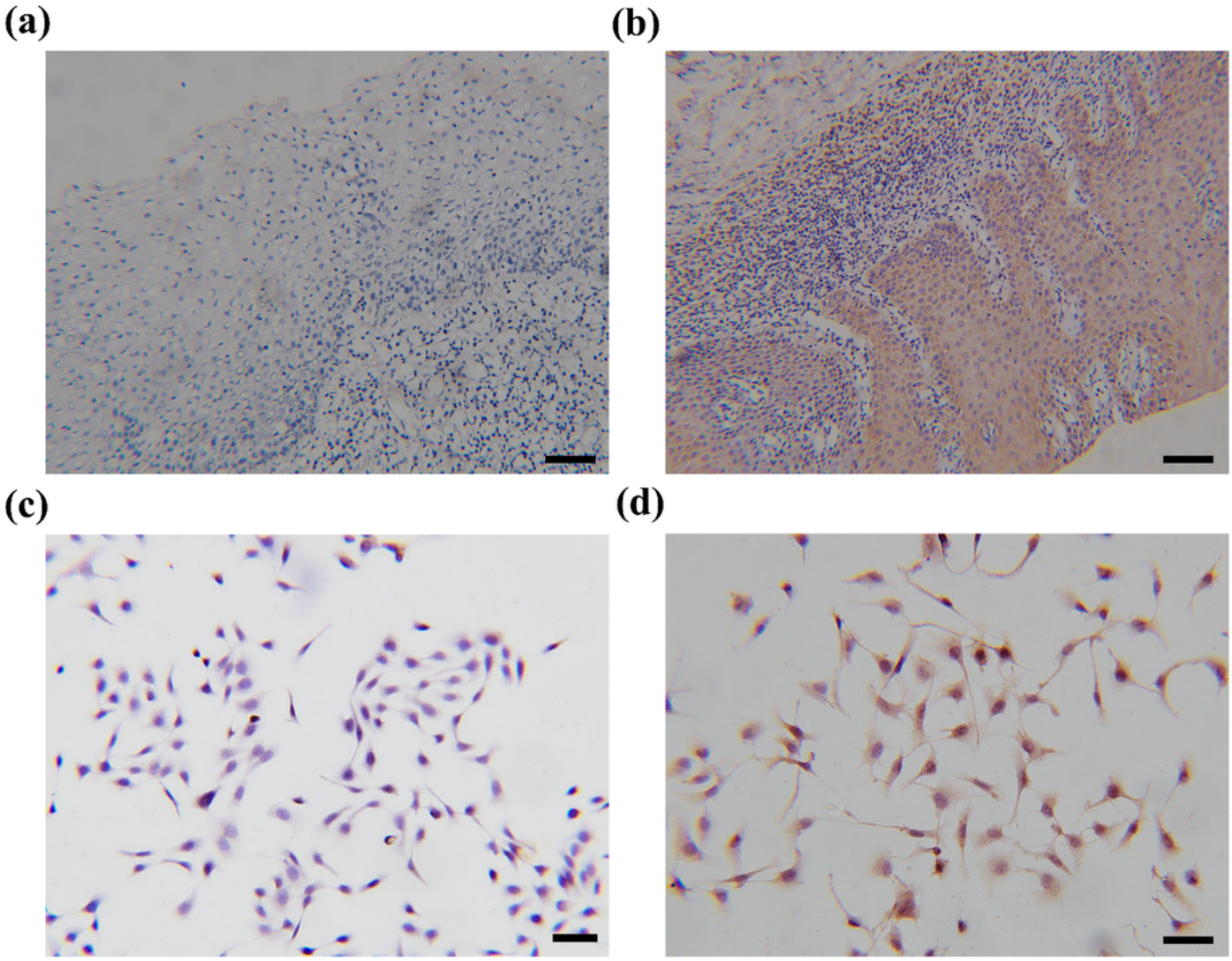

Figure 1

Immunohistochemistry and cellular immunochemistry revealed high expression of FAP in OLK. (a) Localization of FAP in NOM tissues. (b) Localization of FAP in OLK tissues. (c) Localization of FAP in HOK cells. (d) Localization of FAP in HOK tissues. Scale bar: 100 μm

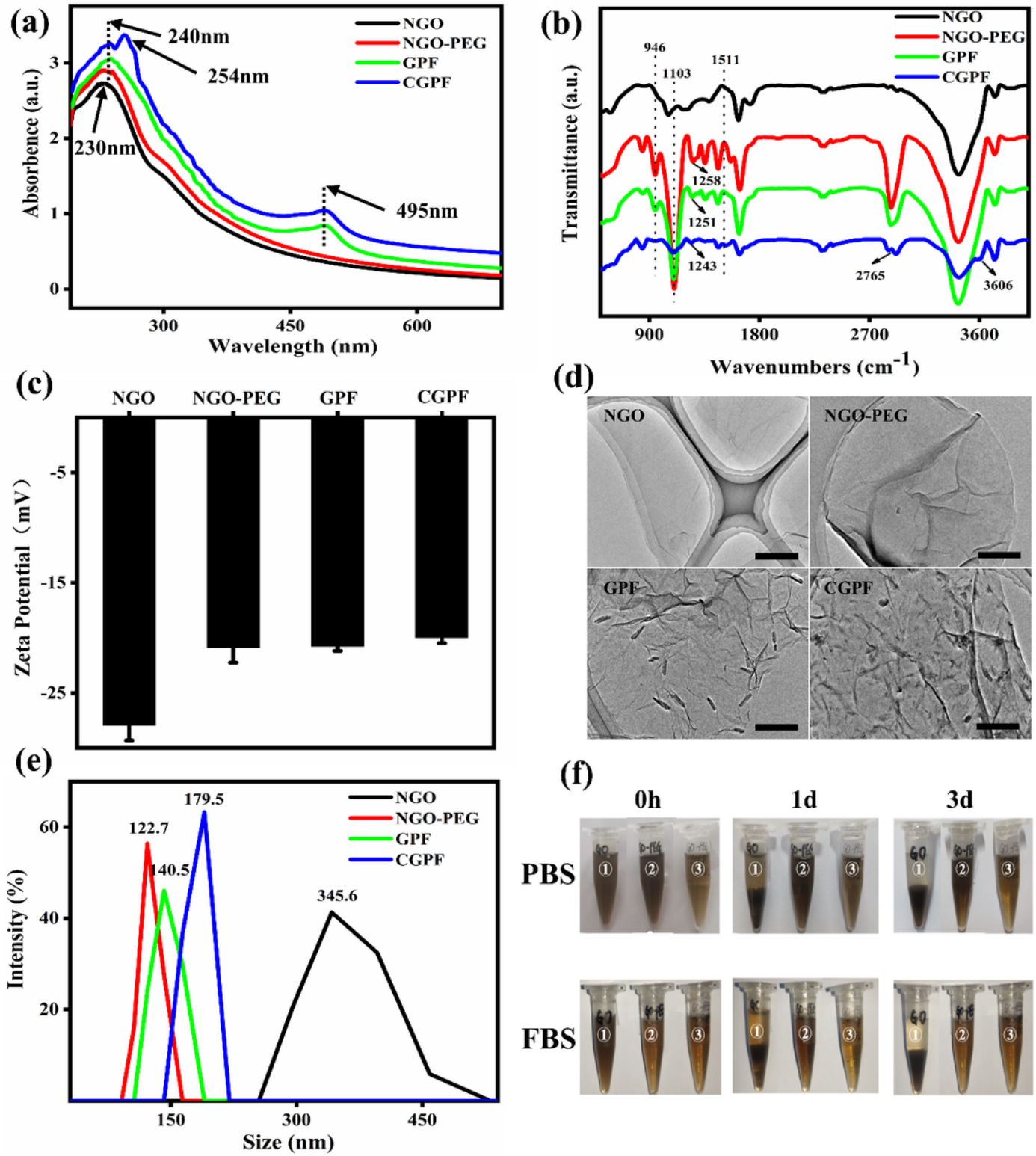

Figure 2

Characterization of CGPF. (a) UV absorbance of NGO, NGO-PEG, GPF, and CGPF. (b) FTIR of NGO, NGO-PEG, GPF, and CGPF. (c) zeta potential of NGO, NGO-PEG, GPF, and CGPF. (d) TEM of NGO, NGO-PEG, GPF, and CGPF,Scale bar:0.5μm. (e) DLS maps of NGO,NGO-PEG, GPF, and CGPF. (f) Stability of NGO, NGO-PEG, and GPF

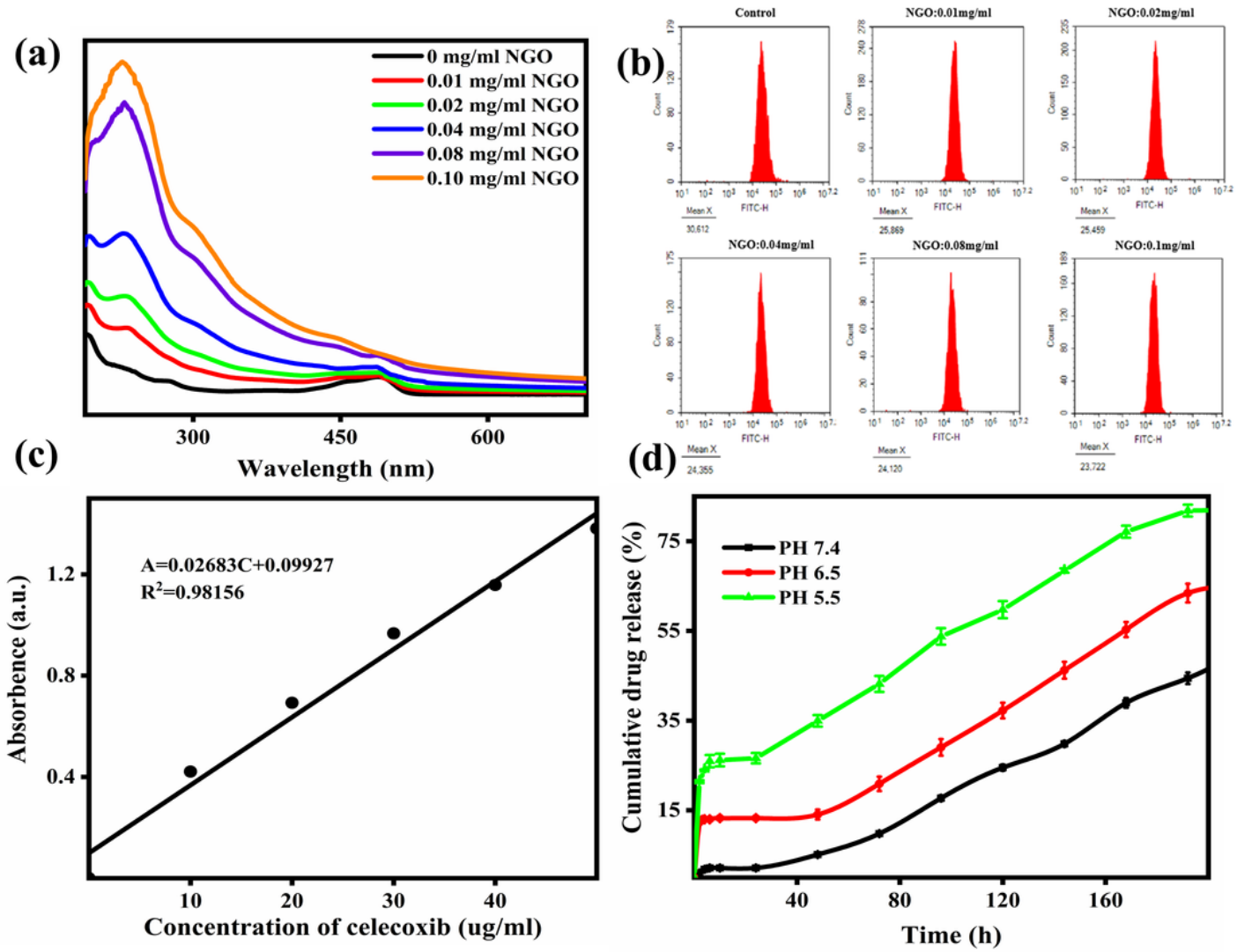

Figure 3

Quenching and recovery of fluorescence, drug loading and release of CGPF. (a) Fluorescence quenching of FAP-targeted peptide fluorescence at different concentrations of graphene. (b) Fluorescence recovery of the probe formed by NGO after incubation with DOK. (c) Standard curve of CXB. (d) In vitro drug-release profile of CGPF at different pH values

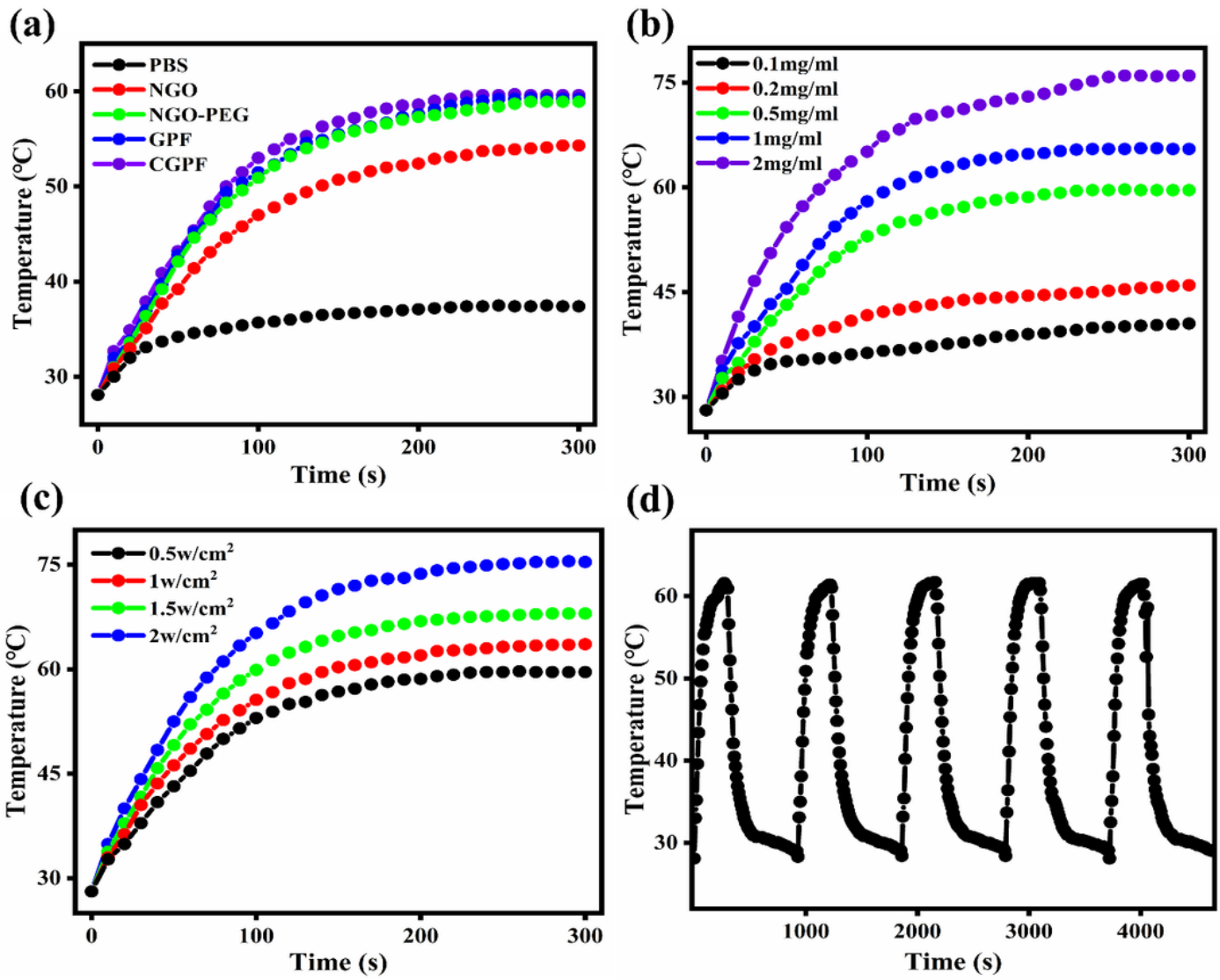

Figure 4

In vitro photothermal effect. (a) Photothermal profile images of PBS, NGO, NGO-PEG, GPF, and CGPF under 808 nm radiation. (b) Photothermal profile images of CGPF aqueous solution with different concentrations under 808 nm radiation. (c) Photothermal profile images of CGPF aqueous solution with different power under 808 nm radiation. (d) Photothermal performance of CGPF over five laser on/off cycles

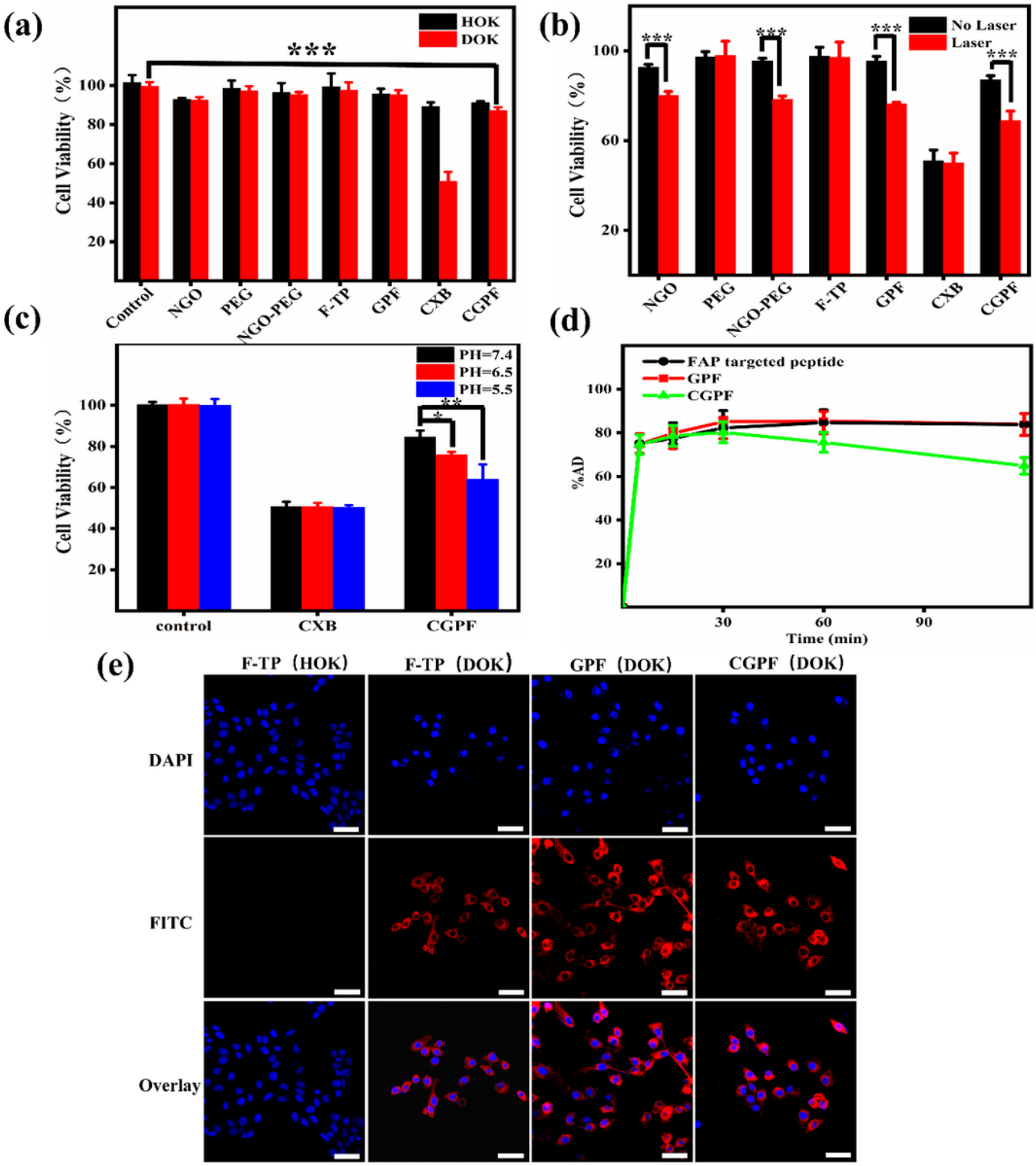

Figure 5

In vitro cytotoxicity and cellular uptake experiments (a) Cellular activity of DOK and HOK cells after treatment with different materials for 24 h. (b) Cellular activity of DOK cells after unphotothermal and photothermal treatments. (c) Cellular activity of DOK cells after treatment with CXB and CGPF at different pH. (d) In vitro cellular uptake studies of F-TP, GPF, and CGPF at 37°C at different times (n = 4, mean ±

SD, *p < 0.05, **p < 0.01,***p < 0.001). (e) Fluorescence images of HOK and DOK cells under F-TP, GPF, and CGPF incubation. Scale bar: 50 μm

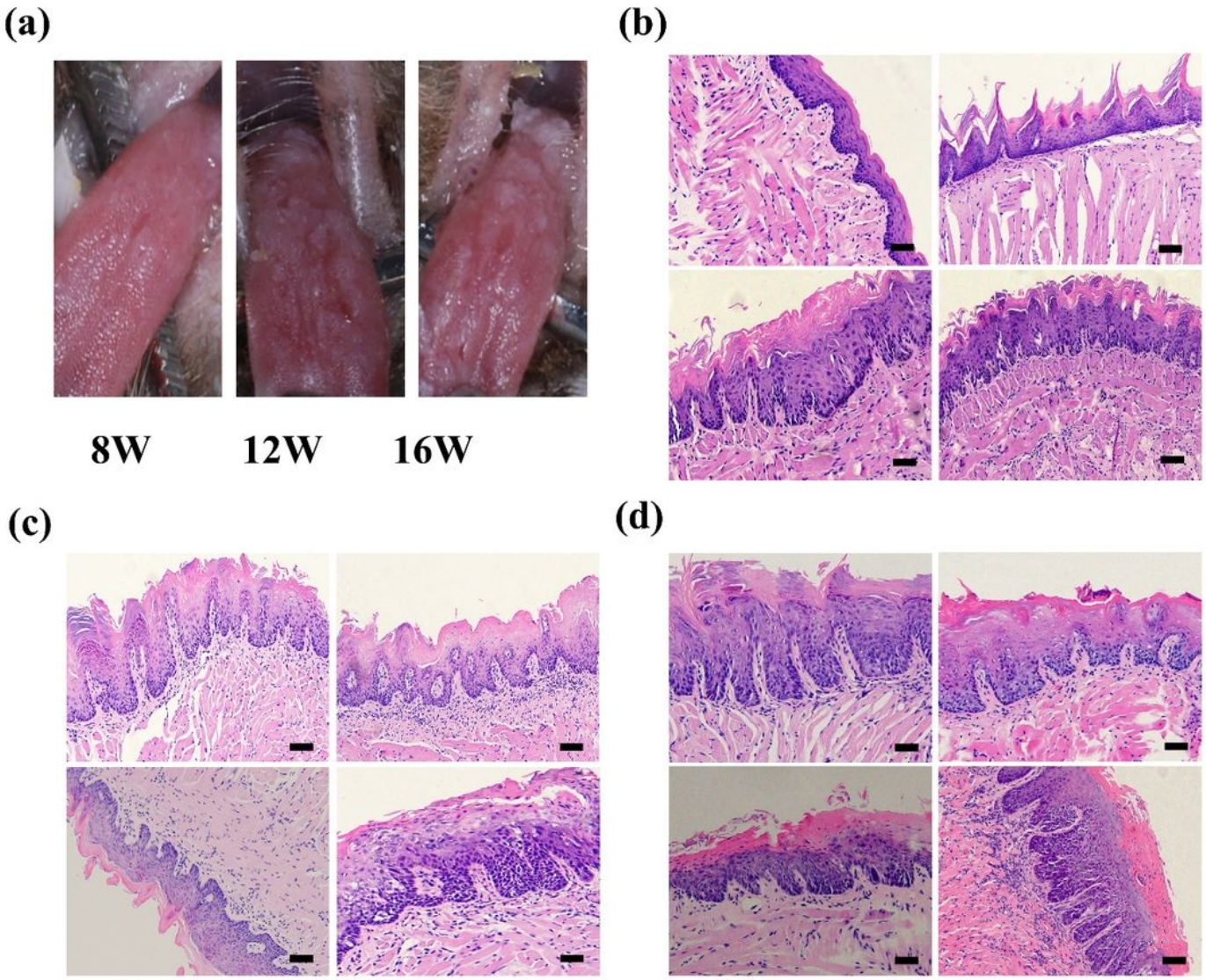

Figure 6

Successful establishment of a mouse OLK model. (a) Representative images of tongues at different administration times. (b) Representative images of HE staining of mouse tongue tissue samples at week

8. (c) week 12, and (d) week 16. Scale bar: 100 μm

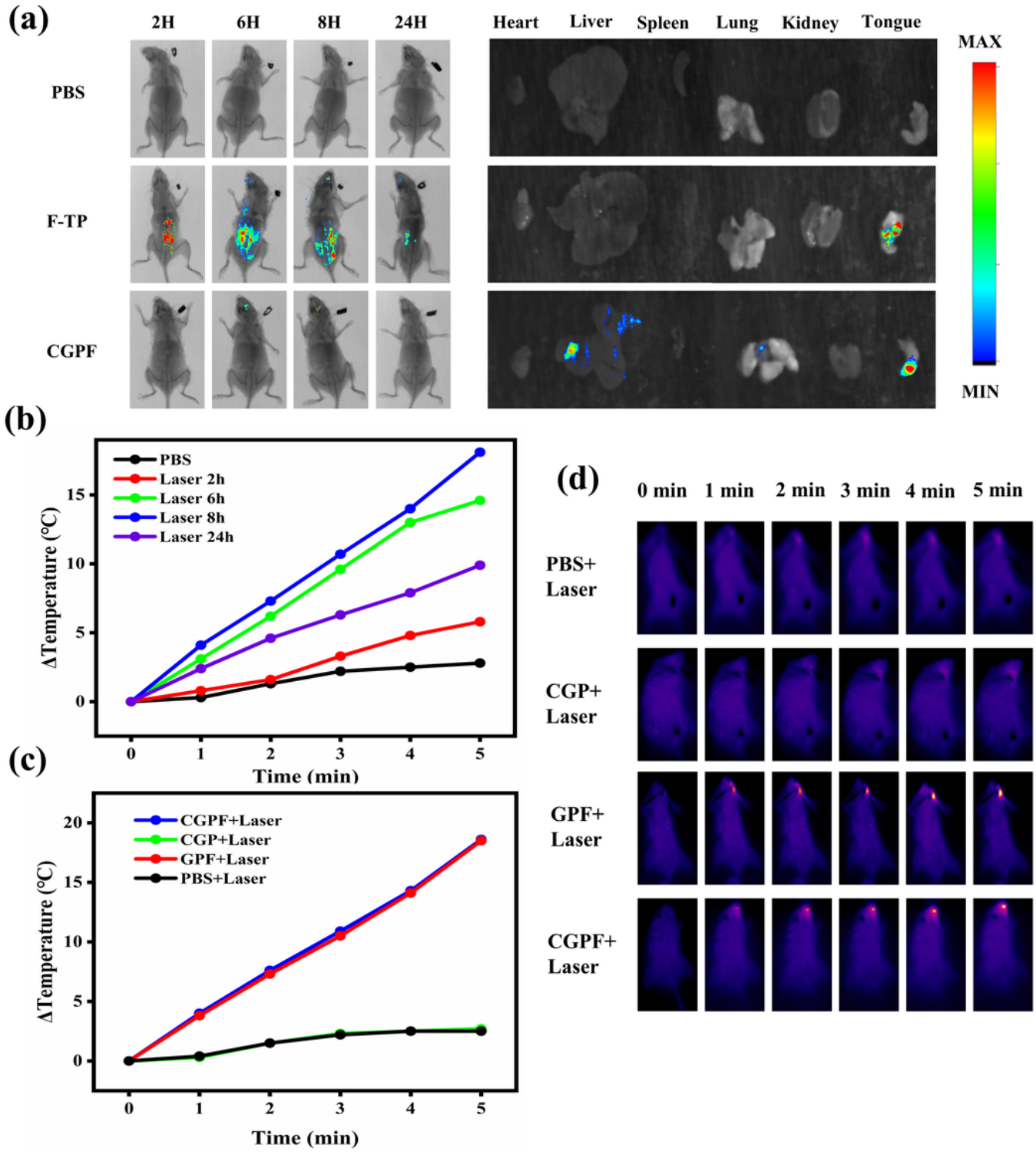

Figure 7

In vivo biodistribution, targeting and photothermal effects (a) In vivo imaging of leukoplakic mice at different time points after intraperitoneal injection of PBS, F-TP, and CGPF, and ex vivo imaging of dissected tumors and major organs at 24 h. (b) Corresponding temperature changes of leukoplakic mice

following the intraperitoneal injection of CGPF under 808 nm laser irradiation at different time points after injection. (c) 808 nm laser irradiation of intraperitoneal injection with corresponding temperature changes in leukoplakic mice injected with PBS, CGP, GPF, and CGPF. (d) Photothermal infrared images of leukoplakic mice injected with PBS, CGP, GPF, and CGPF

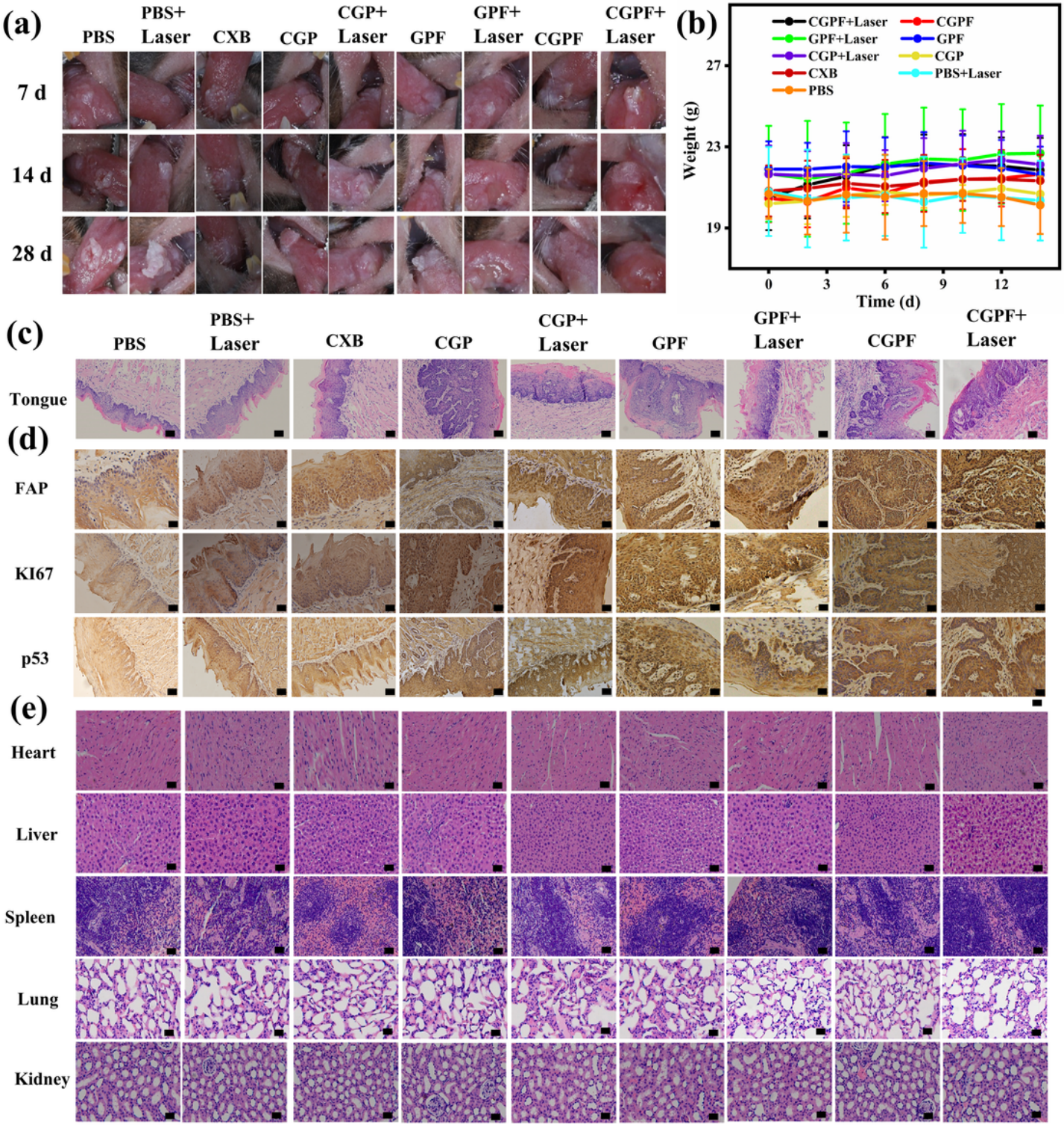

Figure 8

In vivo therapeutic effect and safety assessment of OLK. (a) Performance of tongue lesions in mice on days 7, 14, and 28 after different treatments. (b) Mean body weight of mice in different groups (n=5, mean±standard deviation). (c) Representative histological HE stained images of collected tongue tissues, scale bar = 100 μm. (d) Representative histological images of FAP, KI67, and p53 staining of collected tongue tissues, scale bar = 200 μm. (e) HE stained histological images of major organs after different treatments, scale bar = 100 μm

Supplementary Files

This is a list of supplementary files associated with this preprint. Click to download.

- GraphicalAbstract.png
- Scheme.1.png